Chapter 3

Measurements and Observations of Meteorological Visibility at ITS Stations

Nicolas Hautière, Raouf Babari, Eric Dumont,
Jacques Parent Du Chatelet and Nicolas Paparoditis

Additional information is available at the end of the chapter

http://dx.doi.org/10.5772/55697

1. Introduction

In the presence of dust, smoke, fog, haze or pollution, meteorological visibility is reduced. This reduction constitutes a common and vexing transportation problem for different public authorities in multiple countries throughout the world.

First, low visibility is obviously a problem of traffic safety. Road crashes which occur in fog are generally more severe as the average crash [1]. According to NOAA [2], in the United States there are approximately 700 annual fog-related fatalities, defined as occurring when visibility is less than a $\frac{1}{4}$ mile. Fog constitutes an equally important issue in France, a smaller country, with over 100 annual fatalities attributed to low visibility, defined as occurring when visibility is less than a 400 meters ($\approx \frac{1}{4}$ mile). Indeed, fog causes similar and significant problems on Northern America and French highways. The combination of fog and smoke presence on a motorway was the cause of dramatic pile-ups in France, e.g. on the A10 in 2002 near Coulombiers (58 vehicles involved, 40 injured, 8 deaths). Indeed, even if the origin of both phenomena differs, the combination of their mutual effect on the visibility is exponential, which leads to close to zero visibility areas. It should be stressed that the solution lies not necessarily in better low visibility detection but in drivers' response to fog that they encounter. Indeed, the behavior of drivers in fog is often inappropriate (e.g., reduced headways, altered reaction times) but to understand the origins of these dangerous behaviors is difficult [3]. Different countermeasures have been tested to mitigate the impact of critically reduced visibility [4]. The California San Joaquin and Sacramento Valley regions are particularly adequate test-beds for such measures, because of the well-known Tule fog phenomenon. In the Stockton area of Caltrans District 10, the Caltrans Automated Warning System (CAWS) employs roadside weather stations and visibility meters to provide automated detection [5]. In District 6, Caltrans has installed the "Fog Pilot" system, which

provides a high-technology solution every $\frac{1}{4}$ mile along a 12-mile (20-km) portion of State Route 99.

In addition to the safety problem, reduced visibility is the cause of delays and disruption in air, sea and ground transportation for passengers and freight. On freeways, massive pile-ups create exceptional traffic congestions which sometimes force the operator to momentarily close the road. Fog-related road closures are not an uncommon subject for news headlines. For example, the Heathrow airport was blocked for three days during the 2006 Christmas time. Such events have of course important economic impacts [6]. According to [7], in 1974 fog was estimated to have cost over roughly £120 millions at 2010 prices on the roads of Great Britain. This number includes the cost of medical treatment, damage to vehicles and property, as well as the administrative costs of police, services and insurance, but they do not include the cost of delays to vehicle passengers not directly involved in the accident.

An ability to accurately monitor visibility helps resolve these problems. Important transportation facilities where safety is critical, such as airports, are generally instrumented for monitoring visibility with devices that are expensive and hence, scarce. Cost is precisely the reason why highway meteorological stations are seldom equipped with visibility metering devices. In this context, using already existing and ubiquitous highway cameras is of great interest, as these are low cost sensors already deployed for other purposes such as traffic monitoring [8]. Furthermore, introducing new functionalities into roadside cameras will make them multipurpose and thus more cost-effective, easing their deployment along the roads. In the United States, this potential has been identified by US DOT and was evaluated in the CLARUS Initiative [9], and these efforts may continue with the US DOT IntelliDrive program. In France, a similar initiative has been launched between Ifsttar (French institute of science and technology for transport, development and networks), Météo France (French National Weather Service) and IGN (French National Geographical Institute), three public research institutes dealing with road operation, weather monitoring and forecasting, and geography and cartography, respectively. The French initiative aims at assessing the potential of highway cameras to monitor visibility for different applications ranging from safety hazard detection to air quality monitoring. In the future, such initiatives might make it possible to monitor visibility reduction at the scale of a road itinerary. Prediction, which will soon be possible for airports [10], might even be envisioned.

2. Objectives

2.1. Problematic

Reduced visibility in the atmosphere is directly related to light scattering by air molecules and airborne particles. This tenet of physics is the basis of the operating principle of visibility meters. There are two types of instruments for measuring atmospheric visibility: transmissometers and scatter meters. The transmissometer extrapolates the attenuation of a light beam emitted from a source to a receiver at a known path length in order to estimate the distance for which the emitted light is attenuated by 95%. The transmissometer is also used to calibrate the scatter meter. A scatter meter assesses the dispersion of a light beam at a particular scattering angle, more often close to 40˚(forward-scatter meters). Visibility meters can measure the meteorological visibility distance up to a few tens of kilometers with an error of 20%. The annual statistics on fog occurrence in France, i.e. episodes where the

http://dx.doi.org/10.5772/55697

meteorological visibility distance is lower than 1000 meters are obtained from 60 weather stations distributed over the entire territory. Today, about 160 meteorological stations with visibility measurements are available in real time. But as such, this data cannot be used for predicting fog events and warning road authorities and hence drivers. Indeed, the local nature of this phenomenon is not compatible with the current capacity of meteorological agencies to monitor it accurately. Some studies seek to exploit the photosensitive cells of fixed cameras to measure the visibility.

2.2. The potential of CCTV networks

A survey has been conducted by Météo France on the French motorway networks to estimate the potential of existing CCTV networks to observe the visibility: In 2009, the French motorway network was 8,372 km long and was equipped with approximately 2,000 cameras. Accounting the fact that some are grouped together and some are dedicated to tunnel safety, a potential of 1,000 cameras available to monitor the weather was estimated. The French highway network is also equipped with cameras but they are less numerous. This whole network covers the territory quite uniformly. Consequently, a roadside sensor network constitutes a relevant mesh able to feed meteorological centers with geolocalized data.

2.3. Intelligent Transportation System

The term Intelligent Transportation Systems (ITS) refers to information and communication technology (applied to transportation infrastructure and vehicles) that improves transportation outcomes such as transportation safety, transportation productivity, travel reliability, informed travel choices, social equity, environmental performance and network operation resilience. The recent development of real-time data exchange systems between vehicles and infrastructure allows linking operation centers, roadside sensors and vehicles by means of so-called "ITS Stations". Such technology fosters a new generation of Intelligent Transportation Systems. The objectives of this work is thus to design computer vision methods, which can be implemented into camera-based surveillance systems connected to ITS Stations, in order to detect and characterize reduced visibility conditions, so as to mitigate the risk of accidents by alerting the drivers or by computing adaptive speeds related to the offered visibility distance.

3. Background on meteorological visibility

3.1. Visibility sensor requirements

According to [11, 12], the "meteorological visibility distance" denotes the greatest distance at which a black object of a suitable dimension can be seen in the sky on the horizon, with a threshold contrast set at 5%. The meteorological visibility distance is thus a standard dimension which characterizes the opacity of the atmosphere. According to [13], the road visibility is defined as the horizontal visibility determined 1.2 m above the roadway. It may be reduced to less than 400 m by fog, precipitations or projections. Four visibility ranges are defined and are listed in Tab. 1. Based on these definitions, a visibility sensor should assign the visibility range to one of the four categories and detect the origin of the visibility reduction, i.e. it should detect fog, rain and projections. In this section, the focus is on daytime fog detection and visibility range estimation using two complementary systems.

Visibility range index	Horizontal visibility distance (m)
1	200 to 400
2	100 to 200
3	50 to 100
4	< 50

Table 1. Ranges issued from the French standard NF P 99-320 on highway meteorology, in agreement with the international practice.

3.2. Vision through the atmosphere

The apparent luminance of the road pavement L is given by Koschmieder's law [14] which adds to Beer-Lambert's law a second term corresponding to the atmospheric veil:

$$L = L_0 e^{-kd} + L_f(1 - e^{-kd}) \tag{1}$$

where L_0 denotes the intrinsic luminance of the pavement and L_f the atmospheric luminance. In a foggy image, the intensity I of a pixel is the result of the camera response function crf applied to (1). Assuming that crf is linear, (1) becomes:

$$I = \mathrm{crf}(L) = Re^{-kd} + A_\infty(1 - e^{-kd}) \tag{2}$$

where R is the intrinsic intensity of the pixel, i.e. the intensity corresponding to the intrinsic luminance value of the corresponding scene point and A_∞ is the background sky intensity.

4. Detection and characterization of safety-critical visibility ranges

The first system is able to detect daytime fog and estimate safety-critical visibility ranges. To be run, this system only needs an accurate geometrical calibration of the camera with respect to the road plane.

4.1. Camera modelling

Assuming that the road is locally planar, the distance of a point located at the range d on the roadway can be expressed in the image plane, assuming a pinhole camera model [15]:

$$d = \frac{\lambda}{(v - v_h)} \tag{3}$$

where $\lambda = \frac{H\alpha}{\cos(\theta)}$ and $v_h = v_0 - \alpha \tan(\theta)$. H and θ respectively denote the mounting height and the pitch angle of the camera. $\alpha = \frac{f}{t_p}$ is an intrinsic parameter of the camera based its focal length f and the size t_p of a pixel. v_0 and v_h respectively denote the vertical position in the image of the projection center and of the horizon line (see Fig. 1).

http://dx.doi.org/10.5772/55697

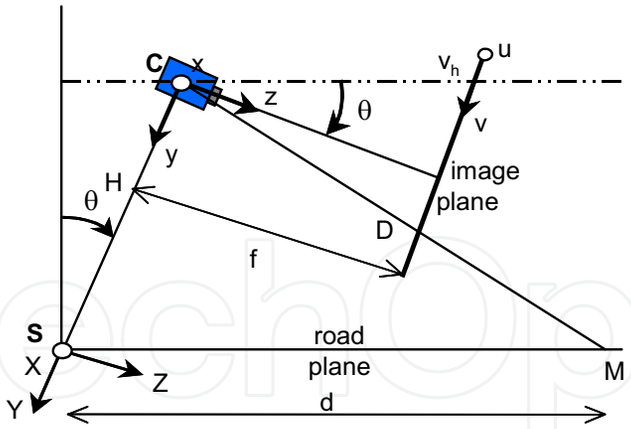

Figure 1. Modelling of the camera within the road environment. v_h: image line corresponding to the horizon line in the image.

The relationship between the distance d on the ground and the distance D from the same point M to the camera is as following:

$$D = \sqrt{H^2 \cos^2\theta + (d - H\sin\theta)^2} \tag{4}$$

4.2. Daytime fog detection

Following a change of d according to v based on (3), (2) then becomes:

$$I(v) = R - (R - A_\infty)(1 - e^{-\frac{k\lambda}{v - v_h}}) \tag{5}$$

By taking the second derivative of I with respect to v, one obtains the following:

$$\frac{\partial^2 I}{\partial v^2}(v) = k\varphi(v)e^{-\frac{k\lambda}{v - v_h}}\left(\frac{k\lambda}{v - v_h} - 2\right) \tag{6}$$

where $\varphi(v) = \frac{\lambda(R - A_\infty)}{(v - v_h)^3}$. The equation $\frac{\partial^2 I}{\partial v^2} = 0$ has two solutions. The solution $k = 0$ is not physically plausible. The only useful solution is (7):

$$k = \frac{2(v_i - v_h)}{\lambda} \tag{7}$$

where v_i denotes the position of the inflection point of $I(v)$. In this manner, if $v_i > v_h$, daytime fog is detected and the parameter k is obtained. We deduce $V_{\text{met}} = \frac{3}{k}$ [11]:

$$V_{\text{met}} = \frac{3\lambda}{2(v_i - v_h)} \tag{8}$$

To implement this principle, a region within the image that displays minimal line-to-line gradient variation when browsed from bottom to top is identified by a segmentation algorithm. A vertical band is then selected in the detected area. Finally, taking the median intensity of each segment yields the vertical variation of the intensity of the image and the position of the inflection point. Details of the method are given in [15]. It has been applied to a sample image in Fig. 2(a). Even if there are many vehicles in the original image, the method is able to ignore them and to detect fog presence, as well as to estimate the meteorological visibility.

4.3. Estimation of the visibility distance

The previous method detects that the visibility is reduced by daytime fog and estimates its density. In the same way, methods dedicated to other meteorological phenomena quantification could be added. Nevertheless, to supervise these different methods, a generic method is needed to estimate the visibility. To achieve this aim, we proposed to compute the distance to the furthest visible object on the road surface. This distance is called the mobilized visibility distance V_{mob}, which is close to the definition of V_{met} if a 5% contrast threshold is chosen [16]. Thus, a local contrast computation algorithm, based on Köhler's binarization technique and described in detail in [16], is applied to the image to compute local contrasts above or equal to 5%. The obtained contrast map contains objects of the road scene. A flat road may be assumed. As a matter of fact, along a top-bottom scanning line of the local contrast map starting from the horizon line, objects encountered get closer to the camera. Consequently, the algorithm consists of finding the highest point in the contrast map having a local contrast above 5%. v_c denotes the corresponding image-line. The distance to this point can then be recovered using Eq. (3), which allows estimating V_{mob} [17]:

$$V_{\text{mob}} = \frac{\lambda}{v_c - v_h} \tag{9}$$

However, the image may also contain vertical objects, which do not respect the flat world assumption and alter the method. This scenario is the case in Fig. 2(b), where the vehicle lights are detected higher in the image than the road surface elements. Another step is thus needed to filter the vertical objects and correctly estimate the visibility distance. This task is achieved using a background modelling method [17].

4.4. Camera specification

First, according to the sensor requirements given in section 3.1, the visibility system shall detect visibility up to d_{max} (400 m in our case). By using Eq. (3), the surface covered by a pixel at the distance d can be computed [15]:

$$\Delta(d) = \frac{\lambda}{\lfloor v_h + \frac{\lambda}{d} \rfloor - v_h} - \frac{\lambda}{\lceil v_h + \frac{\lambda}{d} \rceil - v_h} \tag{10}$$

where $\lfloor x \rfloor$ designates the whole part of x and $\lceil x \rceil$ the integer greater than or equal to x. We proposed this surface to be lower than 10% of d_{max} (40 m in our case), which is a good

http://dx.doi.org/10.5772/55697

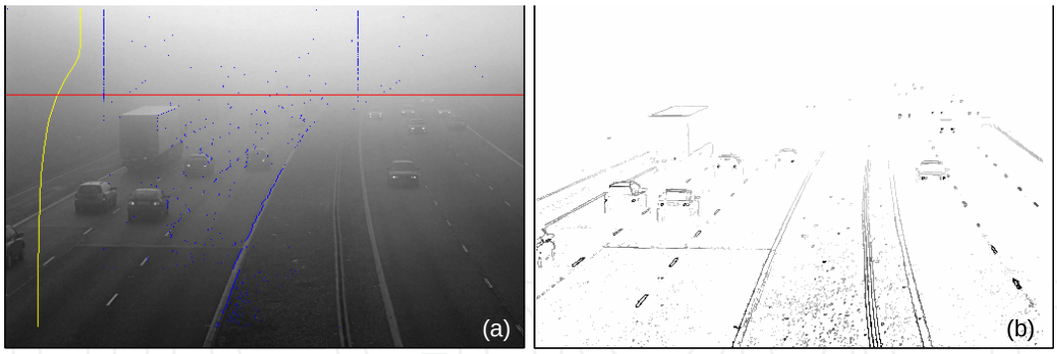

Figure 2. Detection algorithms applied to a fog highway image: (a) The vertical yellow curve represents the instantiation of (2); the horizontal red line represents the estimation of the visibility distance. The blue vertical segments represent the limits of the vertical band analyzed. (b) Map of local contrasts above 5%.

compromise between accuracy and cost [18]:

$$\Delta(d_{\max}) < 0.1 d_{\max} \tag{11}$$

Second, the system must detect fog. Based on section 4.2, the horizon line must lie in the image. Third, the visibility system shall detect visibilities lower than $d_{\min}$ (50 m in our case). To run correctly, the corresponding location of the inflection point must lie in the upper part of the image, i.e. v_i must be lower than v_0. Consequently, additional constraints on the sensor are as following:

$$v_h > 0 \tag{12}$$

$$v_h + \frac{3\lambda}{d_{\min}} < v_0 \tag{13}$$

From (12) and (13), the following inequation is obtained:

$$\sin^{-1}\left(\frac{H}{3d_{min}}\right) < \theta < \tan^{-1}\left(\frac{v_0}{\alpha}\right) \tag{14}$$

The admissible solutions of Eq. (14) can then be used to solve Eq. (11). To fulfill the requirements expressed in [13], we are thus able to specify relevant camera characteristics, which are partly detailed in Tab. 2. In this table, b denotes the diameter of the camera matrix. H denotes the sensor mounting height. f denotes the focal length of the camera optics (see Fig. 1). t_p denotes the pixel size of the camera matrix and dim_y the width of the matrix. θ denotes the pitch angle of the camera.

b [inch]	H [m]	f [mm]	t_p [μm]	dim_y [pix]	θ [degree]
1/2	6	4.5	4.65	1360	28-29

Table 2. Technical solution for camera specification.

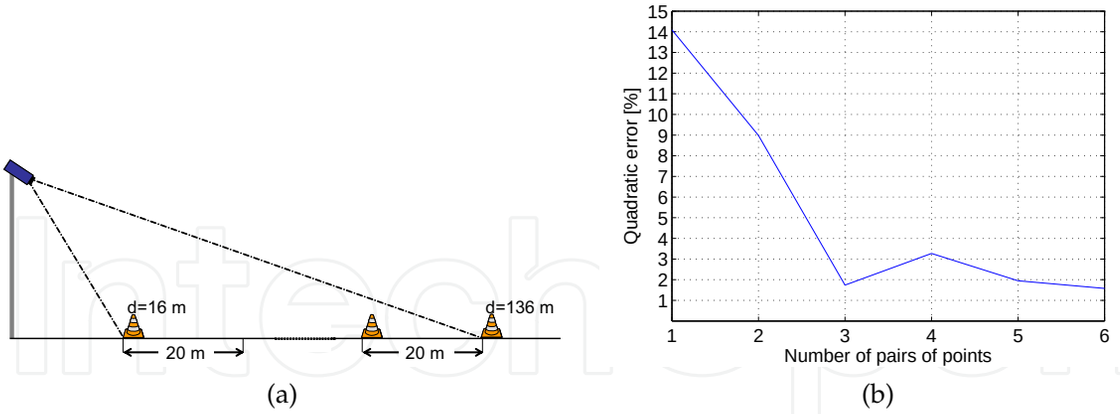

Figure 3. Experimental verification of camera specifications: (a) experimental setup; (b) quadratic error of calibration with respect to the number of considered pairs of points.

4.5. Experimental validation

4.5.1. Verification of Camera Specifications

First, an experimental verification of the camera specifications has been carried out to check if we are able to reach the specifications. To achieve this aim, seven cones were set on a flat road section following the experimental setup of Fig. 3(a). Using the perspective projection model and the positions of the different cones, we are able to calibrate the camera:

$$(\lambda, v_h) = \underset{n=1..7}{\operatorname{argmin}} \sqrt{\sum_{i=1}^{n} \left(d_i - \frac{\lambda}{v_i - v_h} \right)^2} \tag{15}$$

where $\lambda = \dfrac{d_1 - d_n}{\frac{1}{v_1 - v_h} - \frac{1}{v_n - v_h}}$. The quadratic error is plotted in Fig. 3(b) with respect to the number of pairs of points taken into account in the calibration process. Three pairs of points, i.e. four points on the ground, suffice to obtain a quadratic error which is smaller than 2% at $d = 136$ m. This error is in line with the theoretical error at the same distance and hence acceptable.

4.5.2. Implementation of the System

The complete image acquisition system has been installed in a van equipped with a pneumatic pole. Using this vehicle, we have grabbed a sequence of images during sunrise. Sample pictures of this fog episode are shown in Fig. 4(a). The visibility distance has been estimated and is plotted in Fig. 4(b) with respect to the time. As one can see, the visibility distance increases as well as the global illumination in the scene while fog dissipates. The behavior of the system is good except at time $t \approx 50$ min, where the visibility is underestimated. This underestimation is due to the fact that the exposure time is momentarily too high so that the images are overexposed and contrasts deteriorated. Fortunately, the auto-exposure algorithm quickly solves the problem and the visibility increases again up to the maximum value, which is above 400 m as expected.

http://dx.doi.org/10.5772/55697

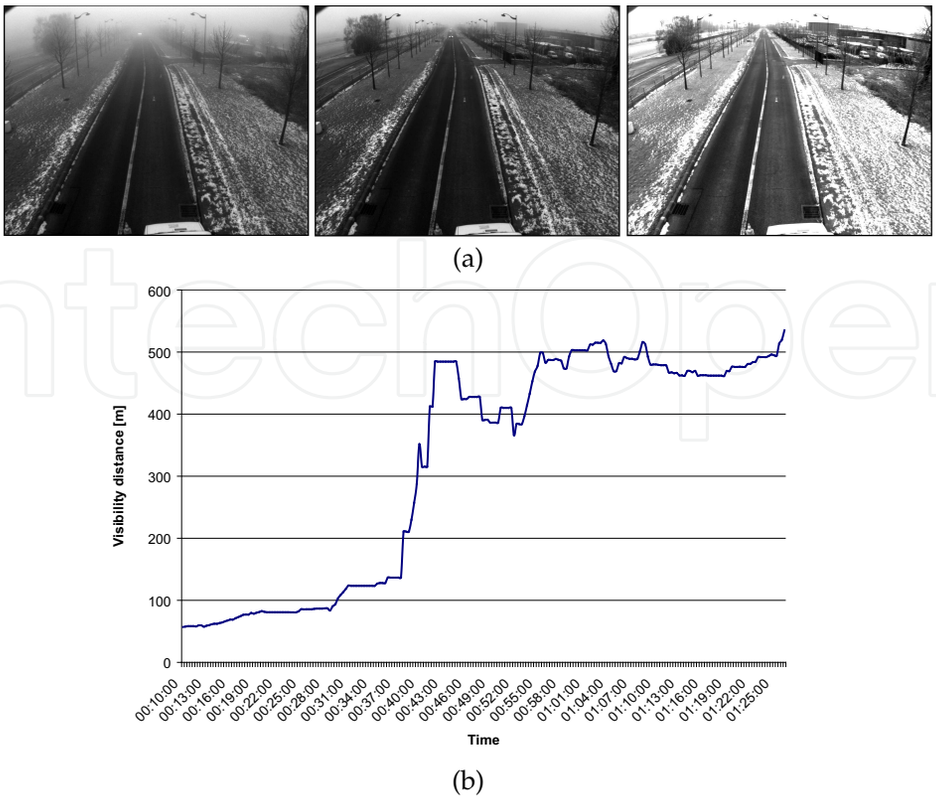

Figure 4. Implementation of the designed camera-based visibility metering system: (a) sample images acquired during a fog episode; (b) visibility distance estimated during this fog episode.

5. Monitoring of meteorological visibility

With the second system, we are able to monitor a whole spectrum of visibility ranges (from 0 to 10,000 m). In this system, we calibrated a response function of the contrast within the image with respect to reference visibility measurements obtained by external sensors. The camera needs not be a high resolution one. However, the calibration is more complex and needs at least one fog episode.

5.1. Contrast of a distant target

Let us consider an outdoor scene where targets are distributed continuously at increasing distances from the camera. When we assume that the surface of the targets is Lambertian, the luminance L at each point i of the target is given by:

$$L = \rho_i \frac{E}{\pi} \tag{16}$$

where E denotes the global illumination and ρ_i denotes the albedo at i. Moreover, it is a classical assumption to set $L_\infty = \frac{E}{\pi}$ so that the contrast of two Lambertian targets at distance d becomes [19]:

$$C = (\rho_2 - \rho_1)e^{-\beta d} \approx (\rho_2 - \rho_1)e^{-\frac{3d}{V}} = \Delta\rho e^{-\frac{3d}{V}} \tag{17}$$

Consequently, the contrast of a distant Lambertian target only depends on its physical properties and on its distance to the sensor and on the meteorological visibility distance, and no longer on the illumination. Such targets allow for computing contrasts in the scene in a way which is robust to strong variations in illumination [19].

5.2. Probabilistic modelling

Let us denote ϕ the probability density function (p.d.f.) of observing a contrast C in the scene:

$$\mathbb{P}(C < X \leq C + \mathrm{d}C) = \phi(C)\mathrm{d}C \tag{18}$$

The expectation of the contrast m in the image is expressed as [19]:

$$m = \mathbb{E}[C] = \int_0^1 C\phi(C)\mathrm{d}C \tag{19}$$

Based on (17), C is a random variable which depends of the two random variables d and $\Delta\rho$. These two variables are assumed to be independent, which allows expressing Eq. (19) as [19]:

$$m = \mathbb{E}\Big[\Delta\rho\Big]\mathbb{E}\Big[e^{-\frac{3d}{V}}\Big] = \overline{\Delta\rho}\int_0^{+\infty}\psi(d)e^{-\frac{3d}{V}}\mathrm{d}d \tag{20}$$

where $\overline{\Delta\rho}$ denotes the mean albedo difference between the objects in the scene and ψ denotes the p.d.f. of there being an object at the distance d in the scene. Choosing a suitable target distribution ψ allows us computing the expectation of the contrast using Eq. (20) with respect to the meteorological visibility distance V.

5.3. Expectation of the mean contrast

In this paragraph, we seek an analytical expression of Eq. (20). To achieve this aim, we assume a scene which contains n Lambertian targets with random albedos located at random distances between 0 and $d_{\max}$. For a given sample scene, we can compute the mean contrast of the targets with respect to the meteorological visibility distance and plot the corresponding curve. Sample curves are plotted in blue in Fig. 5 ($n = 100$ and $d_{\max} = 1000$ m). We can compute the mathematical expectation of the mean contrast and obtain the following analytical model:

$$m_u = \frac{V\Delta\bar{\rho}}{6d_{\max}}\left[1 - \exp\Big(-\frac{3d_{\max}}{V}\Big)\right] \tag{21}$$

where $\Delta\bar{\rho}$ is the mean albedo difference of the targets in the scene. We plot this model in red in Fig. 5. When we do not have any a priori on the targets distribution in the scene, this analytical model is the most probable with which to fit the data [19]. This fact is experimentally assessed in section 5.5. At this stage, we can make a comparison with the charging/discharging of a capacitor. The capacitance of the system is determined by the distribution of Lambertian targets in the scene. The smaller the capacitance of the system is,

http://dx.doi.org/10.5772/55697

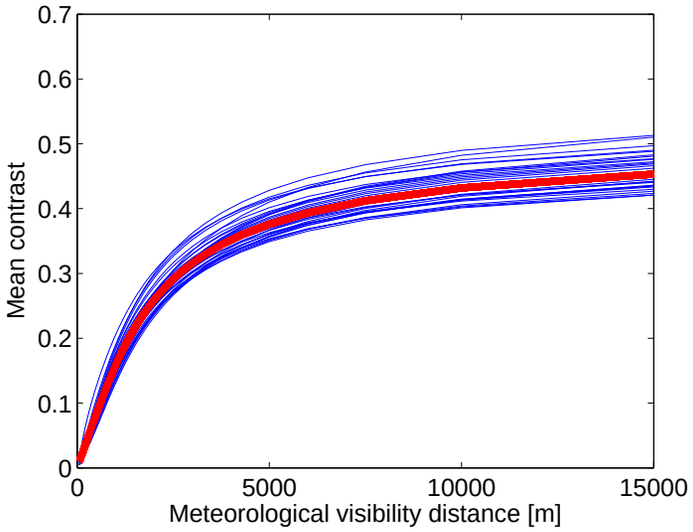

Figure 5. Blue: curves depicting the mean contrast in random scenes with respect to the meteorological visibility distance. Red: expectation of the mean contrast.

the faster the curves reach a 0.5 contrast. We thus define an indicator τ of the system quality which is the meteorological visibility distance at which two thirds of the "capacitance" is reached. A high value of τ also means a lower sensitivity of the model at low meteorological visibility distances.

5.4. Model inversion and error estimation

In the previous section, we have computed an analytical expression of the mean contrast expectation m_u with respect to the meteorological visibility distance V. Ultimately, we would like to compute V as a function of m_u. To achieve this aim, we need to invert the mean contrast expectation function (21). The inversion of this model exists and is expressed by [19]:

$$V(m_u) = \frac{3m_u d_{\max}}{1 + m_u W\left(\frac{e^{\frac{-1}{m_u}}}{m_u}\right)} \tag{22}$$

where the Lambert W function is a transcendental function defined by solutions of $W(x)e^{W(x)} = x$ [20].

5.5. Experimental evaluation

In this section, we present an experimental evaluation of the proposed model for visibility estimation. To achieve this aim, we have collected ground truth data.

5.5.1. Methodology

5.5.1.1. Instrumentation

The observation field test we used is equipped with a reference transmissometer (Degreane Horizon TI8510). It serves to calibrate different scatterometers (Degreane Horizon DF320)

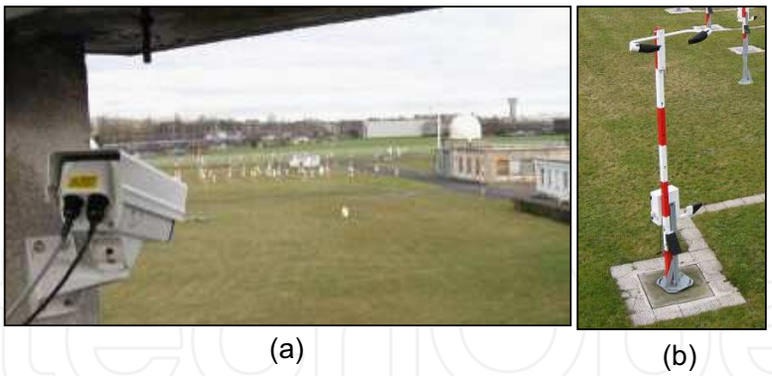

Figure 6. Instrumentation of our observation field test: (a) the camera grabbing pictures of the field test;(b) the scatterometer along with the background luminancemeter.

used to monitor the meteorological visibility distance in France, one of which provided our data. They are coupled with a background luminance sensor (Degreane Horizon LU320) which monitors ambient light conditions. We have added a camera which grabs images of the field test every ten minutes. The camera is an 8-bit CCD camera (640 $\times$ 480 definition, H=8.3 m, $\theta = 9.8^o$, $f_l = 4$ mm and $t_{pix} = 9$ μm). Compared to the camera specified in section 4.4, it is thus a low cost camera which is representative of common video surveillance roadside cameras (cf. section 2.2). Fig. 6(a) shows the installed camera and its orientation with respect to the field test. Fig. 6(b) shows the scatterometer and the background luminancemeter.

5.5.1.2. Data collection.

We have collected two fog events the 28th February and the 1st March 2009. The fog occurred early in the morning and lasted a few hours after sunrise. During the same days, there were strong sunny weather periods. Fig. 7 shows sample images of sunny weather and cloudy weather and foggy weather. The corresponding meteorological visibility distances and luminances are plotted in Figs. 7(d,e). Obviously, the meteorological visibility distance ranges from 100 m to 35.000 m and the luminance ranges from 0 to 6.000 cd.m^{-2}.

We have thus collected exceptional experimental data. Indeed, we met rapidly changing weather conditions over a short period of time. The ranges of meteorological visibility distance and luminance were very large. In the literature, works are dedicated to limited ranges of visibility distances [17, 21]. For example, road safety applications are dealing with 0-400 m [17] whereas people working on environmental issues are dealing with meteorological visibility distances which are above 1000 m [21]. We are among the first to have collected data encompassing both ranges. Moreover, since the data was collected over a short period of time, we consider that the content of the scene did not change. For example, we assumed that the phenology of the trees did not change, so that the amount of texture in the scene without fog remains constant.

5.5.1.3. Location of Lambertian surfaces

To estimate m_u and thus V, we compute the normalized gradient only on the Lambertian surfaces of the scene as proposed in section 5.1. We thus need to locate Lambertian surfaces in the images. To achieve this aim, we compute the Pearson coefficient, denoted $P^L_{i,j}$, between the intensity of pixels in image series where the position of the sun changes and the value of the background luminance estimated by the luminancemeter. The closer $P^L_{i,j}$ is to 1, the stronger

http://dx.doi.org/10.5772/55697

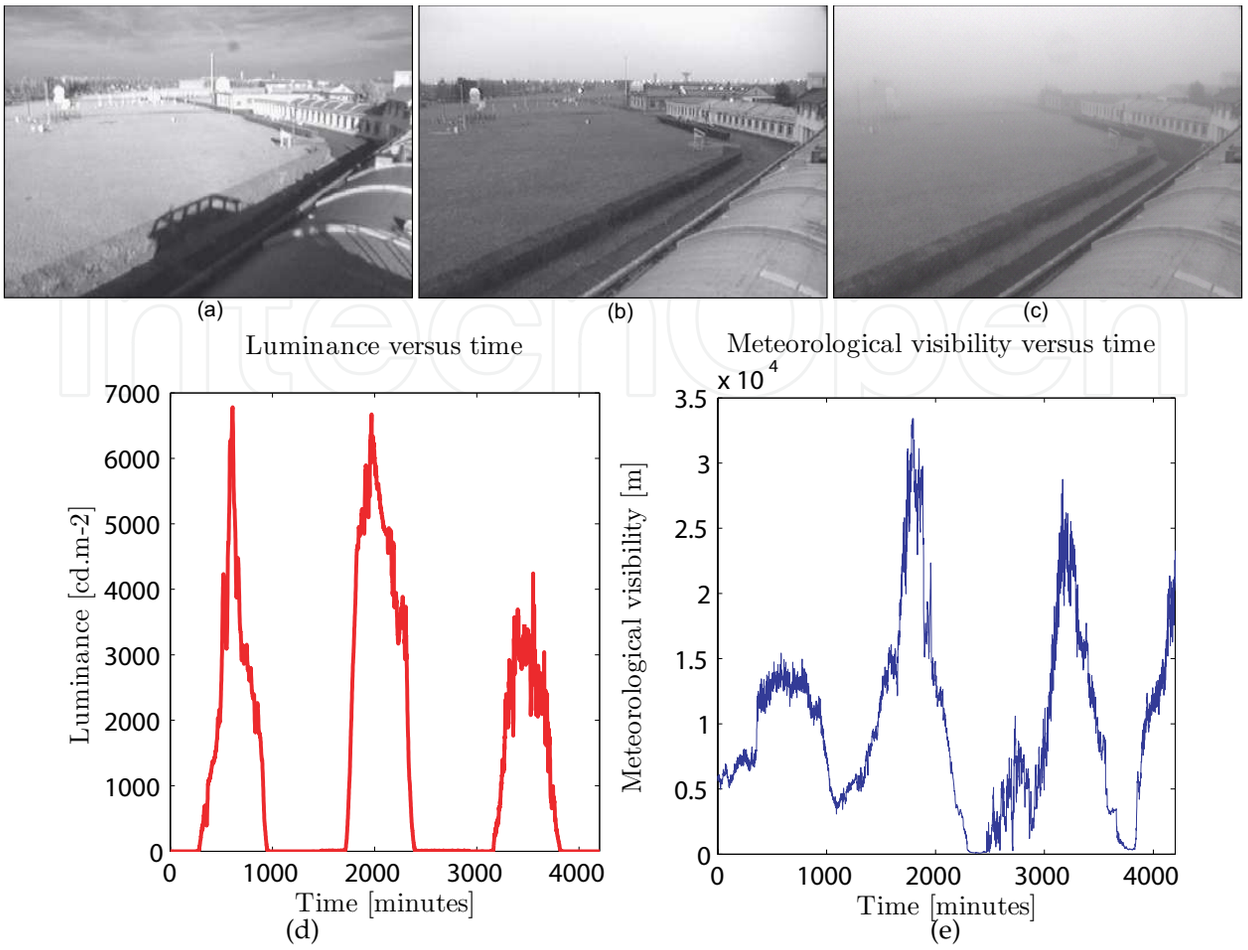

Figure 7. Samples of data collected in winter 2008-2009: (a) images with strong illumination conditions and presence of shadows; (b) cloudy conditions; (c) foggy weather situation; (d) background luminance and (e) meteorological visibility distance data collected in the field test during two days.

Figure 8. Mask of Lambertian surfaces on our field test: The redder the pixel, the higher the confidence that the surface is Lambertian.

the probability that the pixel belongs to a Lambertian surface. This technique provides an efficient way to locate some Lambertian surfaces in the scene. For our field test, the mask of Lambertian surfaces is shown in Fig.8. The redder the pixel, the more the surface is likely to be Lambertian.

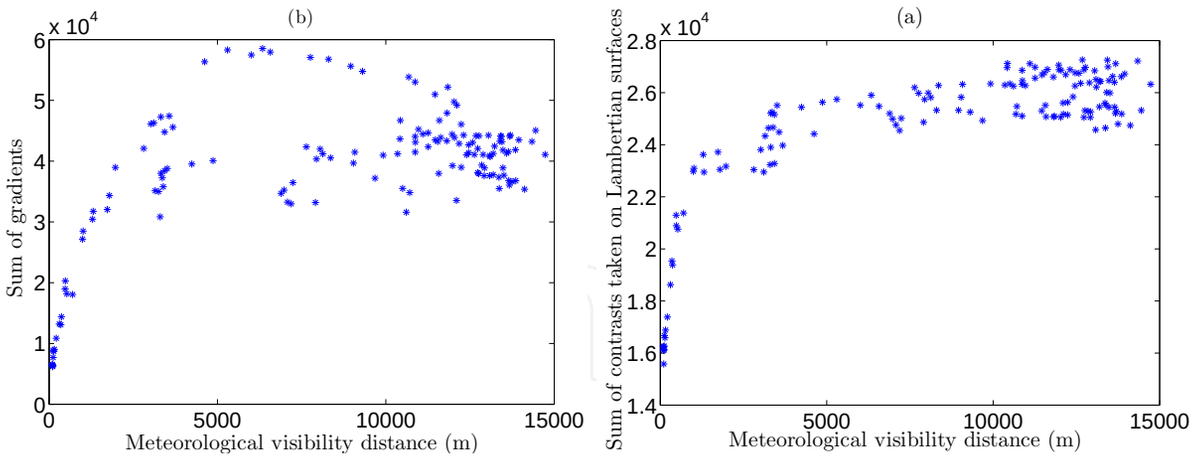

Figure 9. Visibility estimators: (a) the estimator is based on the contrast on Sobel gradient alone; (b) the estimator is based on Sobel gradient weighted by Lambertian surfaces.

Having located the Lambertian surfaces, we can compute the gradients in the scene by means of the module of the Sobel filter. For each pixel, we normalize the gradient $G_{i,j}$ by the intensity of the background. Since our camera is equipped with an auto-iris, the background intensity A_∞ is most of the time equal to $2^8 - 1$, so that this step can be avoided. Each gradient is then weighted by $P^L_{i,j}$, the probability of a pixel to belong to a Lambertian surface where no depth discontinuity exists (P^L is mostly very small). Consequently, only relevant areas of the image are used, and the scene need not be totally Lambertian. Finally, the estimated contrast in the scene $\tilde{m_u}$ is given by [19]:

$$\tilde{m_u} = \sum_{i=0}^{h}\sum_{j=0}^{w} \Delta\rho_{i,j} \exp\left(-\frac{3d_{i,j}}{V}\right) \approx \sum_{i=0}^{h}\sum_{j=0}^{w} \frac{G_{i,j}}{A_\infty} P^L_{i,j} \tag{23}$$

where $\Delta\rho_{i,j}$ is the intrinsic contrast of a pixel in Eq. (17), and h and w are respectively the height and the width of the images.

5.5.2. Results

5.5.2.1. Contrast estimators

We have computed Eq. (23) for our collection of 150 images with different meteorological visibility distances. For comparison purposes, we have also computed the simple sum of gradients in the image without weighting the Lambertian surfaces. The results are shown in Fig. 9. By using the Lambertian surfaces, we can see that the shape of the distribution in Fig. 9(a) looks like the curve proposed in Fig. 5, which is very satisfactory. Conversely, when all the pixels of the scene are used, the points are more scattered when the meteorological visibility distance is above 2500 m (see Fig. 9(b)): When the sky is clear and the visibility is high, the illumination from the sun strongly influences the gradients in the scene. Consequently, the estimation of the visibility is altered. These two distributions show the benefit of selecting the Lambertian surfaces to estimate the visibility distance.

http://dx.doi.org/10.5772/55697

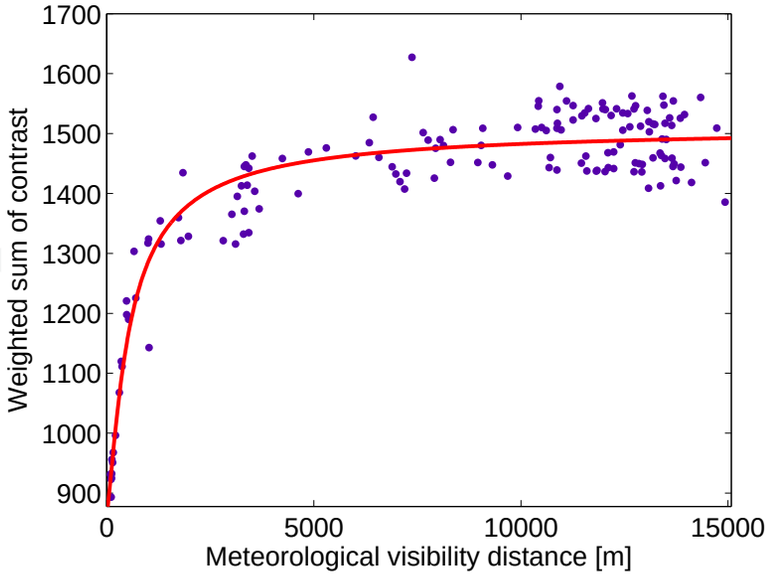

Figure 10. Data fitting with the mean contrast model. Dots: data. Red curve: fitted model.

5.5.2.2. Model fitting

We have to fit the mean contrast model (Eq. (21)) to the data shown in Fig. 9(a) using robust regression techniques. To ensure a mathematical solution, we have fitted the model (Eq. (24)), which is slightly different from the theoretical model. Three unknown variables a, b and d_{max} have to be estimated, which can be easily done using classical curve fitting tools.

$$\tilde{m_u} = \frac{aV}{d_{\max}}\left[1 - \exp\left(-\frac{3d_{\max}}{V}\right)\right] + b \tag{24}$$

This model fits well with the data ($R^2 = 0.91$). In particular, we obtain $d_{\max} = 307.2$ m. The fitted curve is plotted in Fig. 10. We estimated a capacitance (as defined in section 5.3) of the system $\tau \approx 950$ m.

5.5.2.3. Discussions

From the fitted model, we can now invert the model using (22) and estimate the meteorological visibility distance $\tilde{V}$ based on the mean contrast m_u[19]:

$$\tilde{V} = \frac{3d_{\max}(b - m_u)}{(b - m_u)W\left(\frac{ae^{\frac{a}{b-m_u}}}{b - m_u}\right) - a} \tag{25}$$

After having estimated the meteorological visibility distance, we can compute the error on this estimation. The results are given in Tab. 3. Since the applications are very different depending on the range of meteorological visibility distances, we have computed the error and the standard deviation for various applications: road safety, meteorological observation and air quality. One can see that the error remains low for critical safety applications. It

increases for higher ranges of visibility distances, and becomes huge for visibility distances above 7 km. Different issues may be discussed. First, the model presented in this chapter is relevant for uniform distributions of distances which happen in many environments, such as highway scenes. The scene in which the experimental data used in this paper were collected may be meet this assumption. Second, the Sobel operator is certainly not the best estimate for the gradient. Indeed, it is a simple high-pass filter which is problematic because of the impulse noise of camera sensors. Different filters may be used to enhance the images beforehand, or to compute the contrast more robustly.

6. Outcome

First, a camera-based system has been developed to detect safety-critical visibility conditions. Sample results based on data collected during a morning fog episode are shown in the Fig. 4. When visibility is below 400 m, the accuracy of the system is expected to be 90%. The second system has been assessed on the test site of Météo France in Trappes, where images have been grabbed with visibility data (see Fig. 7). Based on our experiments, we are able to obtained error estimates which are lower than 10% [19] as well.

We thus have at disposal two different techniques to estimate the visibility distance in case of fog or haze. The first technique is dedicated to low visibility ranges but needs a high-resolution camera along with a simple calibration process. The second technique is not restricted to low visibility ranges and works with a low cost camera but needs a more complex calibration procedure. It is clear that the complementarity between both approaches must be studied so as to build a single system, which is easy to set up and deploy.

7. Potential applications

7.1. Winter maintenance

The monitoring of meteorological visibility has different applications for winter maintenance [22]. First, the knowledge of a low visibility area is important for the safety of winter maintenance operations. Second, a sudden drop of the visibility can be due to heavy snow falls. The relationship between liquid equivalent snowfall rate and visibility has also been investigated [23], which means that a camera-based visibility meter is potentially a good snow sensor. Finally, meteorological models have been developed to forecast pavement temperatures as well as snow height [24]. Nebulosity and fog are phenomena which alter the prediction, since the radiative transfer between the pavement and the air is affected. The assimilation of visibility data in these prediction models may be useful to increase the accuracy of forecasts.

Application	Highway fog	Meteorological fog	Haze	Air quality
Range [m]	0-400	0-1000	0-5000	0-15000
Number of data	13	19	45	150
Mean error [%]	12.6	18.1	29.7	-
Std [%]	13.7	18.9	22	-

Table 3. Relative errors of meteorological visibility distance estimation with respect to the envisioned application.

http://dx.doi.org/10.5772/55697

7.2. Fog nowcasting

The forecasting of the weather within the next six hours is often referred to as nowcasting. In this time range, it is possible to forecast smaller features such as individual showers and thunderstorms with reasonable accuracy, as well as other features too small to be resolved by a computer model. [25] show that combining satellite-based forecasting of low clouds with terrestrial measurements of humidity allows computing a probability of fog occurrence. A camera-based visibility meter could easily substitute for a humidity sensor. Indeed, using camera-based visibility estimation and meteorological data, [26] showed that visibility can be predicted up to 15 minutes in advance with 1-km mesh meteorological data. Such camera-based nowcasting methods may be good solutions to allow the re-routing of vehicles before they reach a low-visibility area in a timely manner.

7.3. Pile-up prevention and mitigation

[27] has proposed a review of best practices in terms of mitigation of highway visibility problems, in particular fog related issues. In this paper, he describes existing installations in the USA dedicated to driver alert in case of low visibility on the highway. Apart from fog dispersal techniques, the best practices are related to the timely alert of the drivers which approach a foggy area. Then, depending on the fog density, different advisory speed limits may be posted. In the same time, the public lighting is adapted. The component of these systems are made of weather stations, CCTV cameras and Variable Message Signs (VMS). More recently, Caltrans has installed the "Fog Pilot" system in District 6, which provides a high-technology solution every $\frac{1}{4}$ mile along a 12-mile (20-km) portion of State Route 99. This centralized solution relies on the use of infrastructure to vehicle communications to warn the drivers whose vehicles are equipped with a receiver, in case of sudden low speed area. Thanks to the proposed camera-based visibility monitoring techniques, we are able to build a decentralized fog-pilot, which makes use of CCTV cameras to monitor the visibility and allows optimizing the speed of drivers approaching a low visibility area, as well as the intensity of road studs. Based on best existing practices, its principle is to warn the drivers of a foggy area with enough time, so that they can adapt their speed to the prevailing visibility distance in the dangerous area.

8. Conclusion and perspectives

Reliable solutions to accurately monitor the meteorological visibility along road networks at reasonable costs are still not available. The use of the cameras, which are multifunctional sensors and are already deployed along the roadsides, is a promising solution. However, progress in computer vision are still needed to obtain robust techniques, which are able to fulfill the needs of transportation safety, of meteorology and of environment in terms of observation.

In this chapter, we have presented two different camera-based systems to estimate the visibility distance. These systems could be integrated in ITS stations to alert drivers as well public authorities in case of fog hazard. The first system is dedicated to safety-critical visibility ranges but needs a high-resolution camera along with a simple calibration process. The second technique is not restricted to low visibility ranges and needs a low cost camera but a more complex calibration procedure. In the future, it is obvious that the

complementarity between both approaches must be studied so as to build a single system, which will be easy to set up and to deploy. Second, the problem of night fog is still subject to research. In particular, we would like to adapt our in-vehicle techniques of night fog detection to visual surveillance. Third, we would like to develop an intelligent camera where fog detection is implemented along with existing traffic applications (virtual loops, AID, etc.). Finally, we would like to develop test beds for our sensing technologies and our decentralized fog-pilot.

Author details

Nicolas Hautière[1], Raouf Babari[1], Eric Dumont[1],
Jacques Parent Du Chatelet[2] and Nicolas Paparoditis[3]

1 Université Paris-Est, Institut Français des Sciences et Technologies des Transports, de l'Aménagement et des Réseaux, France
2 Météo France, France
3 Université Paris-Est, Institut Géographique National, France

References

[1] M. Abdel-Aty, A.-A. Ekram, H. Huang, and K. Choi. A study on crashes related to visibility obstruction due to fog and smoke. *Accident Analysis and Prevention*, 43:1730–1737, 2011.

[2] B. Whiffen, P. Delannoy, and S.. Siok. Fog: Impact on road transportation and mitigation options. In *National Highway Visibility Conference, Madison, Wisconsin, USA*, May 2004.

[3] J. Kang, R. Ni, and G. J. Andersen. Effects of reduced visibility from fog on car-following performance. *Transportation Research Record: Journal of the Transportation Research Board*, (2069):9–15, 2008.

[4] F.D. Shepard. *Reduced Visibility Due to Fog on the Highway*. Number 228. 1996.

[5] C. A. Mac Carley. Methods and metrics for evaluation of an automated real-time driver warning system. *Transportation Research Record: Journal of the Transportation Research Board*, (1937):87–95, 2005.

[6] T. Pejovic, V. A. Williams, R. B. Noland, and R. Toumi. Factors affecting the frequency and severity of airport weather delays and the implications of climate change for future delays. *Transportation Research Record: Journal of the Transportation Research Board*, (2139):97–106., 2009.

[7] A. H. Perry and L. J. Symons. *Highway Meteorology*. University of Wales Swansea, Swansea, Wales, United Kingdom, 1991.

[8] N. Jacobs, Burgin W., N. Fridrich, A. Abrams, K. Miskell, B. Brswell, A. Richardson, and R. Pless. The global network of outdoor webcams: Properties and apllications. In *ACM International Conference on Advances in Geographic Information Systems*, 2009.

http://dx.doi.org/10.5772/55697

[9] R. Hallowell, M. Matthews, and P. Pisano. An automated visibility detection algorithm utilizing camera imagery. In *23rd Conference on Interactive Information and Processing Systems for Meteorology, Oceanography, and Hydrology (IIPS), San Antonio, TX, Amer. Meteor. Soc.*, 2007.

[10] S. Roquelaure, R. Tardif, S. Remy, and T Bergot. Skill of a ceiling and visibility local ensemble prediction system (leps) according to fog-type prediction at paris-charles de gaulle. *Airport. Weather and Forecasting*, 24:1511–1523, 2009.

[11] CIE. *International Lighting Vocabulary*. Number 17.4. 1987.

[12] WMO. *Guide to Meteorological Instruments and Methods of Observation*. Number 8. World Meteorological Organization, 2008.

[13] AFNOR. Road meteorology - gathering of meteorological and road data - terminology. NF P 99-320, April 1998.

[14] W.E.K. Middleton. *Vision through the atmosphere*. University of Toronto Press, 1952.

[15] N. Hautière, J.-P. Tarel, J. Lavenant, and D. Aubert. Automatic fog detection and estimation of visibility distance through use of an onboard camera. *Machine Vision Applications*, 17(1):8–20, 2006.

[16] N. Hautière, R. Labayrade, and D. Aubert. Real-time disparity contrast combination for onboard estimation of the visibility distance. *IEEE Transactions on Intelligent Transportation Systems*, 7(2):201–212, June 2006.

[17] N. Hautière, E. Bigorgne, and D. Aubert. Visibility range monitoring through use of a roadside camera. In *IEEE Intelligent Vehicles Symposium*, 2008.

[18] J.D. Crosby. Visibility sensor accuracy: what's realistic? In *12th Symposium on Meteorological Observations and Instrumentation*, 2003.

[19] N. Hautière, R. Babari, E. Dumont, R. Brémond, and N. Paparoditis. *Lecture Notes in Computer Science, Computer Vision - ACCV 2010*, volume 6495, chapter Estimating Meteorological Visibility using Cameras: A Probabilistic Model-Driven Approach, pages 243–254. Springer, March 2011.

[20] R. M Corless, G. H. Gonnet, D. E. G. Hare, D. J. Jeffrey, and D. E. Knuth. On the Lambert W function. *Advances in Computational Mathematics*, 5:329–359, 1996.

[21] C.-H. Luo, C.-Y. Wen, C.-S. Yuan, C.-C. Liaw, J.-L. ans Lo, and S.-H. Chiu. Investigation of urban atmospheric visibility by high-frequency extraction: Model development and field test. *Atmospheric Environment*, 39:2545–2552, 2005.

[22] Y. Nagata, T. Hagiwara, K. Araki, Y. Kaneda, and H. Sasaki. Application of road visibility information system to winter maintenance. *Transportation Research Records: Journal of the Transportation Research Board*, 2055:128–138, 2008.

[23] Jothiram Vivekanandan Jeffrey Cole Barry Myers Charles Masters Rasmussen, Roy M. The estimation of snowfall rate using visibility. *Journal of Applied Meteorology and Climatology*, 38(10):1542–1563, 1999.

[24] L. Bouilloud, E. Martin, F. Habets, A. Boone, P. Le Moigne, J. Livet, M. Marchetti, A. Foidart, L. Franchistéguy, S. Morel, J. Noilhan, and P. Pettré. Road surface condition forecasting in france. *Journal of Applied Meteorology and Climatology*, 48(12):2513–2527, 2009.

[25] V. Guidard and D. Tzanos. Analysis of fog probability from a combination of satellite and ground observation data. *Pure and Applied Geophysics*, 164:1207–1220, 2007.

[26] N. Yasuhiro, T. Hagiwara, K. Takitani, F. Kawamura, Y. Kaneda, and M. Sakai. Development of a visibility forecast model based on a road visibility information system (RVIS) and meteorological data. In *Transportation Research Board Annual Meeting, Washington DC, USA*, number Paper 11-2342, 2011.

[27] N. McLawhorn. Mitigating highway visibility problems. In *National Highway Visibility Conference*, 2004.